Vis Geosci (2006) 9: 49–57
DOI 10.1007/s10069-004-0020-7

ORIGINAL ARTICLE

Bijaya B. Karki · Ravi Chennamsetty

A visualization system for mineral elasticity

Received: 14 July 2004 / Accepted: 30 September 2004 / Published online: 5 November 2004

Abstract The authors have developed an efficient visualization system to gain insight into large collections of mineral elasticity data produced by an increasing number of both theoretical calculations and experiments. The system allows us to visualize multivariate elastic moduli (i.e., elastic constant tensors) and their variation with composition, pressure and temperature. Moreover, it supports visualization of elastic wave propagation in an anisotropic medium by rendering the wave velocity data, which are calculated as a function of propagation direction in a three-dimensional space. This paper describes the design, implementation and application of the visualization scheme we have developed for mineral elasticity. In particular, our scheme exploits a combination of parallel coordinates, star plot, scatter plot and polygon-surface rendering techniques, which are implemented using OpenGL, GLUI and C++. The result is a highly portable and flexible interactive visualization system. For illustration, the elastic properties of several important oxide and silicate minerals are successfully visualized as a function of pressure and temperature.

Keywords Elasticity · Mantle minerals · High pressure · Seismology · Scientific visualization

Introduction

Over the past several years, numerous experiments and theoretical calculations have been carried out to investigate the elastic properties of a wide range of solid materials. The resulting massive datasets are crucial to our understanding of processes ranging from brittle failure, to flexure, to the propagation of elastic waves that occur in a solid medium. One of the areas where the study of elasticity is very common and important is related to the Earth's interior. The elasticity of the materials that are believed or known to make up the Earth's interior is key to interpreting seismological observations in terms of chemical, thermal and dynamical states of the planet. The elastic wave velocities of minerals and mineral assemblages at high pressure-temperature conditions are often compared with seismic velocities measured as a function of depth to place tighter constraints on the composition at depth. Knowledge about the elastic anisotropy of the component minerals is essential for understanding the relationship between seismic anisotropy and dynamics (e.g., mantle flow).

Experimental measurements of the elastic properties at elevated pressures and temperatures are increasingly common and precise for minerals (e.g., Liebermann and Li 1998; Sinogeikin et al. 2004). Added to the experiments are theoretical approaches such as those which are based on first principles quantum mechanical theory and widely used to accurately predict the mineral elasticity at conditions encompassing the entire pressure-temperature regime of the Earth's interior (e.g., Karki et al. 2001; Oganov et al. 2001; Wentzcovitch et al. 2004). The resulting large collections of data (see The Elle Mineral Properties Database 2004) are important to address fundamental issues related to the elasticity: How the elasticity behaves across different materials (for instance, tetrahedrally and octahedrally coordinated oxides and silicates—thought to be the major building blocks of the Earth's mantle) and how sensitive it is to variations in pressure and temperature. It has been shown that the acoustic anisotropy of the major mantle phases varies from zero to more than 50% and depends on pressure strongly (in some cases nonmonotonically). Compression is also known to have a strong effect on the elasticity through pressure-induced structural phase transitions in several systems. Extracting such information from the available massive multivariate elasticity

Reviewed by: D. Yuen, G. Erlebacher

B. B. Karki (✉) · R. Chennamsetty
Department of Computer Science,
Louisiana State University,
Baton Rouge, LA 70803, USA
E-mail: karki@bit.csc.lsu.edu
Fax: +1-225-5781465

dataset is, however, a non-trivial task; and there is still the lack of an efficient mechanism for doing this.

In this paper, we adopt a visualization approach to facilitate understanding of various aspects of mineral elasticity datasets. Scientific visualization has recently emerged as an attractive approach to gaining insight into a variety of datasets in the geosciences for useful, meaningful information (e.g., Dzwinel et al. 2003; Erlebacher et al. 2001, 2002; Wang et al. 2003). In essence, visualization is a process of transforming and mapping of the abstract physical data/information into some visual (graphical) form (Schroeder et al. 1997). Our aim is to develop an efficient scheme that enables an interactive visualization of the elastic properties of minerals for their potential implications in materials physics and geophysics. Here, we report the design, implementation and application of the recently developed elasticity visualization system.

Design and implementation

In particular, we focus on visualization of the multivariate elastic moduli and anisotropic elastic wave propagation. Our visualization scheme consists of two components; namely, data processing (e.g., generation of additional data wherever needed) and rendering (mapping data into interactive graphical forms). A combination of parallel coordinates, star plot, scatter plot and polygon-surface rendering techniques are exploited to graphically represent the data. Implementation is done with a combination of OpenGL (Woo et al. 1999; www.opengl.org), GLUI (http://www.cs.unc.edu/~rademach/glui) and C++. The result is a platform independent and flexible interactive visualization system design. Figure 1 lists different modules of our visualization system and their functions.

Visualization of elastic moduli

The elasticity of a crystal is characterized by a multivariate physical quantity (ideally a fourth rank tensor) called the elastic constant tensor, $C_{\alpha\beta\gamma\sigma}$ (with $\alpha, \beta, \gamma, \sigma = 1, 2, 3$) (Musgrave 1970). There are 81 independent components in general, however, this number is reduced to 21 by the requirement of Voigt symmetry (Voigt 1928). In Voigt notation, the elastic constants form a symmetric 6×6 matrix, C_{ij} with $i,j = 1, 2 \ldots 6$. The presence of crystal symmetry further reduces the number of independent C_{ij}'s. The highest possible symmetry is that of an isotropic material such as a glass or randomly oriented polycrystalline aggregate, which is fully characterized by two elastic constants (bulk and shear

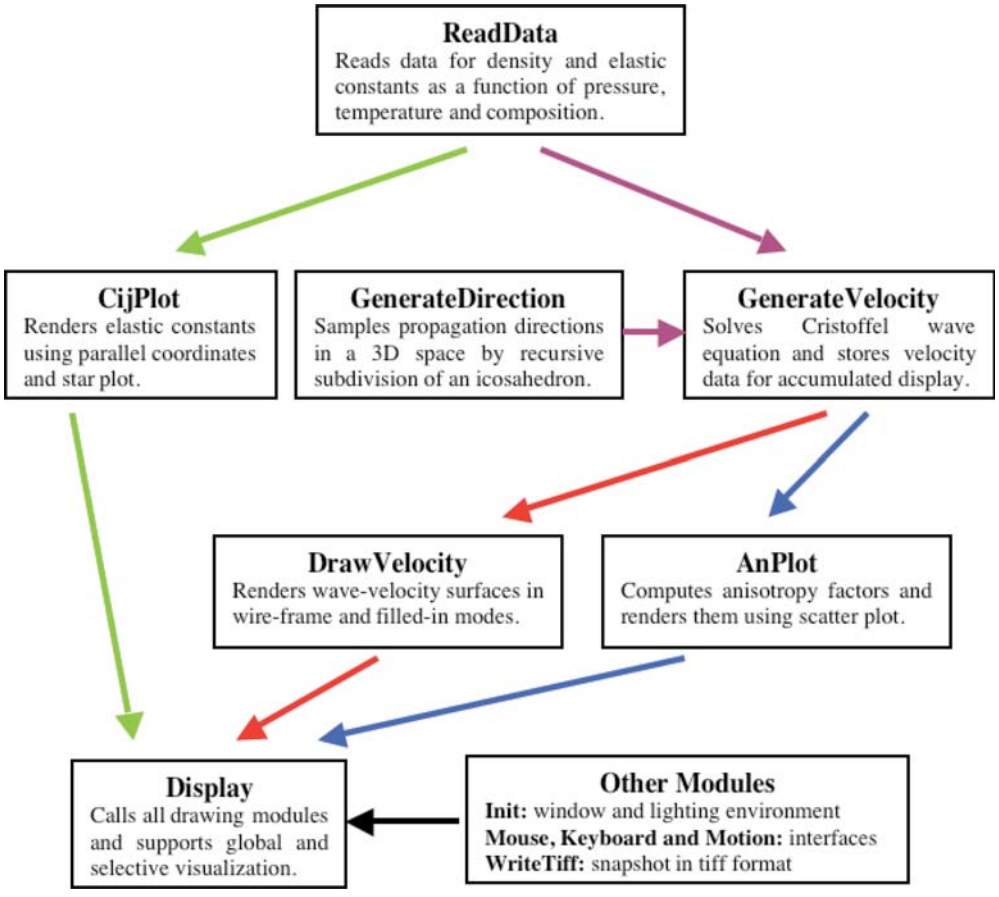

Fig. 1 Different modules of the visualization system. *Arrows* indicate the relationships among the modules, e.g., CijPlot() uses input data from ReadData() and supplies objects to Display()

modulus). A cubic crystal is characterized by three constants, C_{11}, C_{12} and C_{44}. Crystals with lower symmetry possess higher number of independent constants, for example, nine for orthorhombic crystal and 21 for triclinic crystal (the largest number possible for a crystalline solid). One can divide the elastic constants of a given system into different groups, namely, longitudinal-, shear- and mixed-elastic constants. Visualization of the elastic moduli datasets will assist us to study the relationships among different elastic constants in terms of their types and magnitudes and to understand the effects of composition, pressure and temperature on elastic moduli.

We adopt the parallel coordinates and star plot techniques to visualize the C_{ij} data as these techniques are widely used for multivariate data visualization (see Schroeder et al. 1997). In both techniques, the number of axes is equal to the number of independent elastic constants, which is determined by the symmetry of the mineral under consideration; for example, an orthorhombic crystal will have nine axes. However, the layout of the axes in the two cases is different; in parallel coordinates, the axes are drawn vertically parallel and equally spaced whereas in star plot, the axes radiate at equal angle intervals from a common point (origin). In the cases, where the elastic moduli of minerals of different symmetries are displayed together, the number of the axes is determined by the lowest crystal symmetry. In Figs. 2 and 3, which illustrate the visualization of the data at ambient conditions for several minerals (primarily, oxides and silicates) of cubic, hexagonal, tetragonal and orthorhombic symmetries taken from The Elle Mineral Properties Database (2004), nine axes corresponding to an orthorhombic symmetry are used. The data points are marked on different axes and then connected with color-coded straight lines. Different colors represent different symmetries; black for cubic, green for hexagonal, red for tetragonal and blue for orthorhombic. The intensity of each color is varied to represent different minerals within each symmetry class. Color-coding is also used to display elastic constants as a function of pressure or temperature.

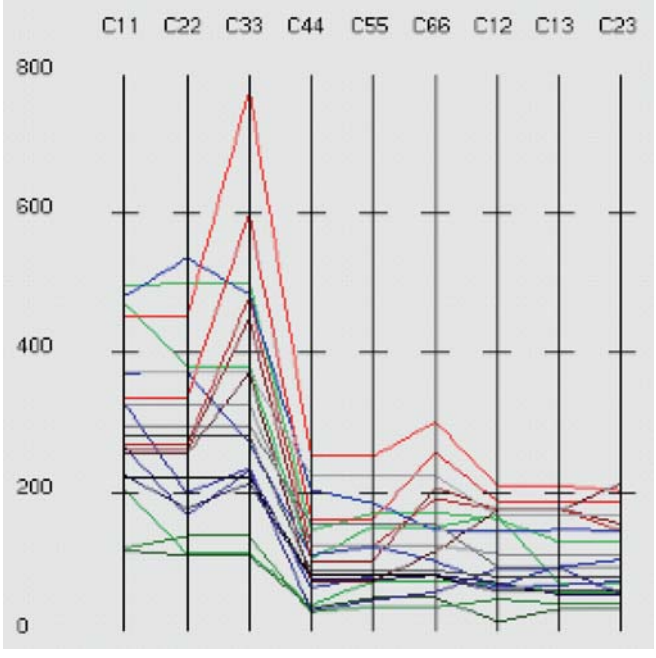

Fig. 2 Parallel coordinates: visualization of the elastic moduli of 20 minerals, which are grouped into four sets according to crystal symmetry; cubic (*black*), hexagonal (*green*), tetragonal (*red*) and orthorhombic (*blue*)

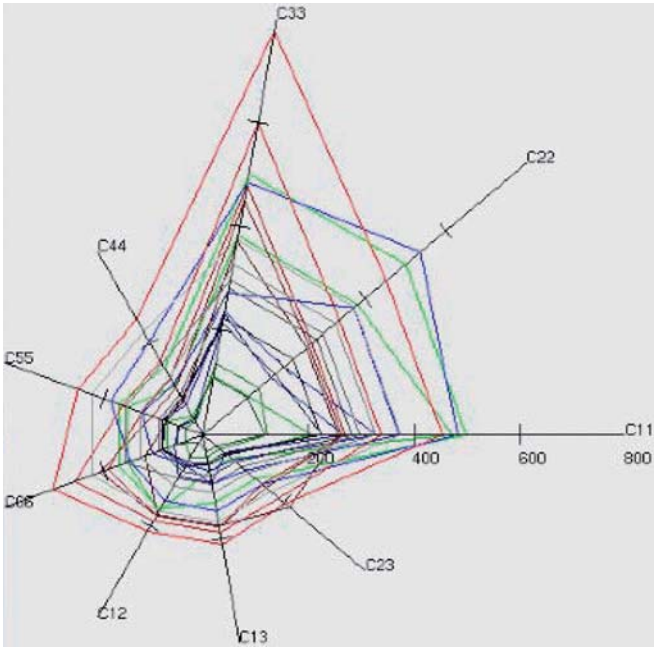

Fig. 3 Star plot: visualization of the elastic moduli of 20 minerals. The colors have the same meanings as in Fig. 2

Visualization of elastic wave propagation

Because the elastic constant tensor is fourth-ranked, all crystals are elastically anisotropic regardless of symmetry. One consequence is that the elastic wave velocities depend on the direction of propagation. The elastic wave

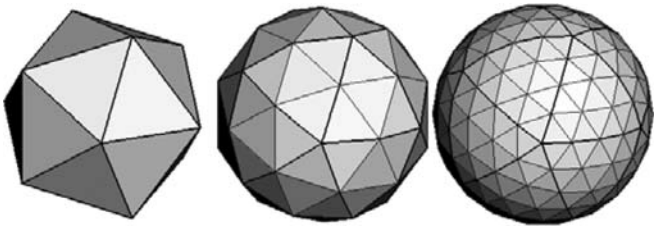

Fig. 4 Using icosahedron to generate a fine set of the wave propagation directions in 3D space

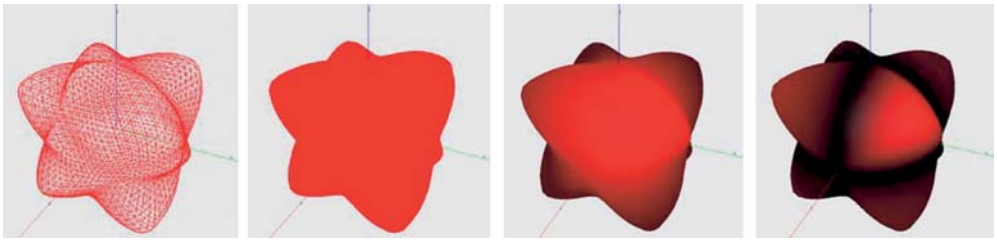

Fig. 5 A typical wave velocity surface rendered in a wire-frame mode (*left*) and in various filled-in polygon modes that include solid coloring with lighting disabled, shading (*lighting enabled*) and scaled coloring (*from left to right*)

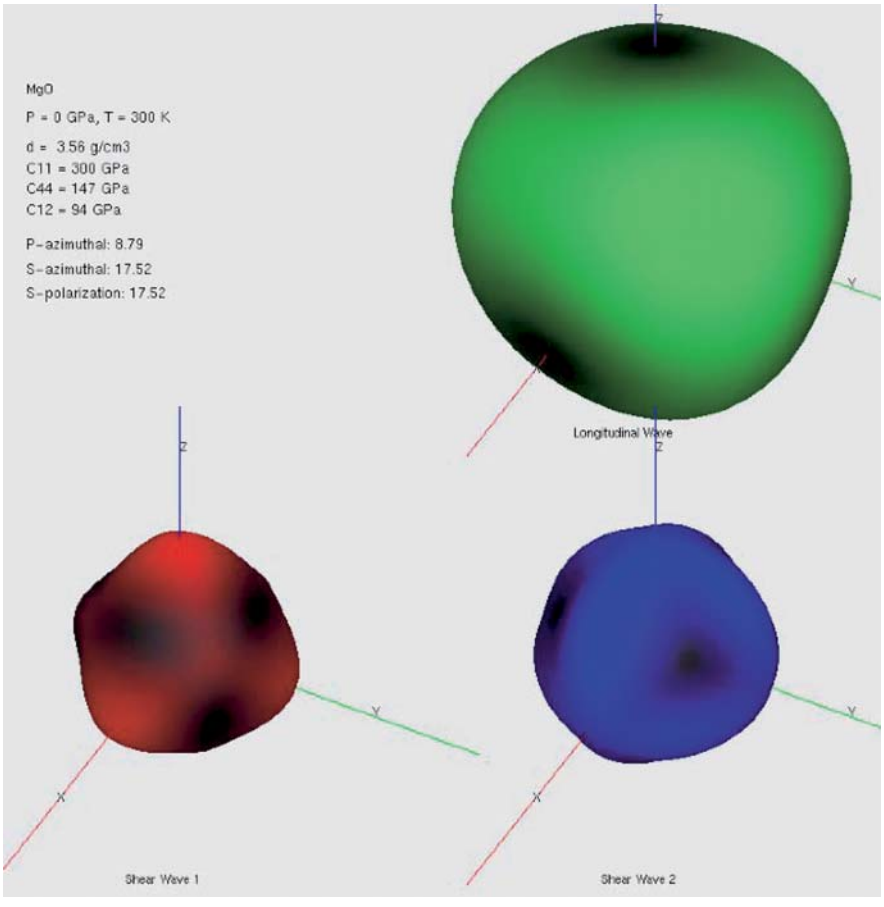

Fig. 6 Visualization of three velocity-direction distributions: green longitudinal (*P*), red for one shear wave (*S1*) and blue for the other shear wave (*S2*). The data used are for MgO (Karki et al. 1999)

propagation is determined by the Cristoffel equation (Musgrave 1970):

$$\left|C_{\alpha\beta\gamma\sigma}n_\beta n_\sigma - \rho V^2\delta_{\alpha\gamma}\right| = 0$$

where n is the propagation direction, ρ is the density, V is the velocity and δ is the Kroenecker delta function. The eigenvalues yield the three unique wave velocities and the eigenvectors yield the polarization directions. The solutions are of two types: a quasi-longitudinal wave with polarization nearly parallel to the propagation direction, and two quasi-shear waves with polarization nearly perpendicular to the direction. In seismology, the quasi-longitudinal wave is usually referred to as the primary (P) or compressional wave and the quasi-transverse waves as secondary (S) or shear waves, the former propagating faster than the latter. Pure longitudinal and shear polarizations are found only along special high symmetry propagation directions in anisotropic materials. The visualization of wave propagation in an anisotropic material involves (a) generation of velocity-direction data using the Cristoffel equation and (b) subsequent graphical representation of the data.

A fine sampling of propagation directions of unit length, which are of uniform distribution, radiating from a point in a 3D space is generated using an icosahedron as the basis for a unit sphere. Note that an icosahedron approximates a spherical surface in terms of triangles (Fig. 4). Thus the lines joining the centre and vertices on the surface of the icosahedron (i.e., radial directions) represent propagation directions. Initially, our icosahedron has only 12 triangles thereby resulting in only 20 directions. The number of propagation directions is increased by recursively subdividing the triangles to add more vertices on the surface and calculating directional

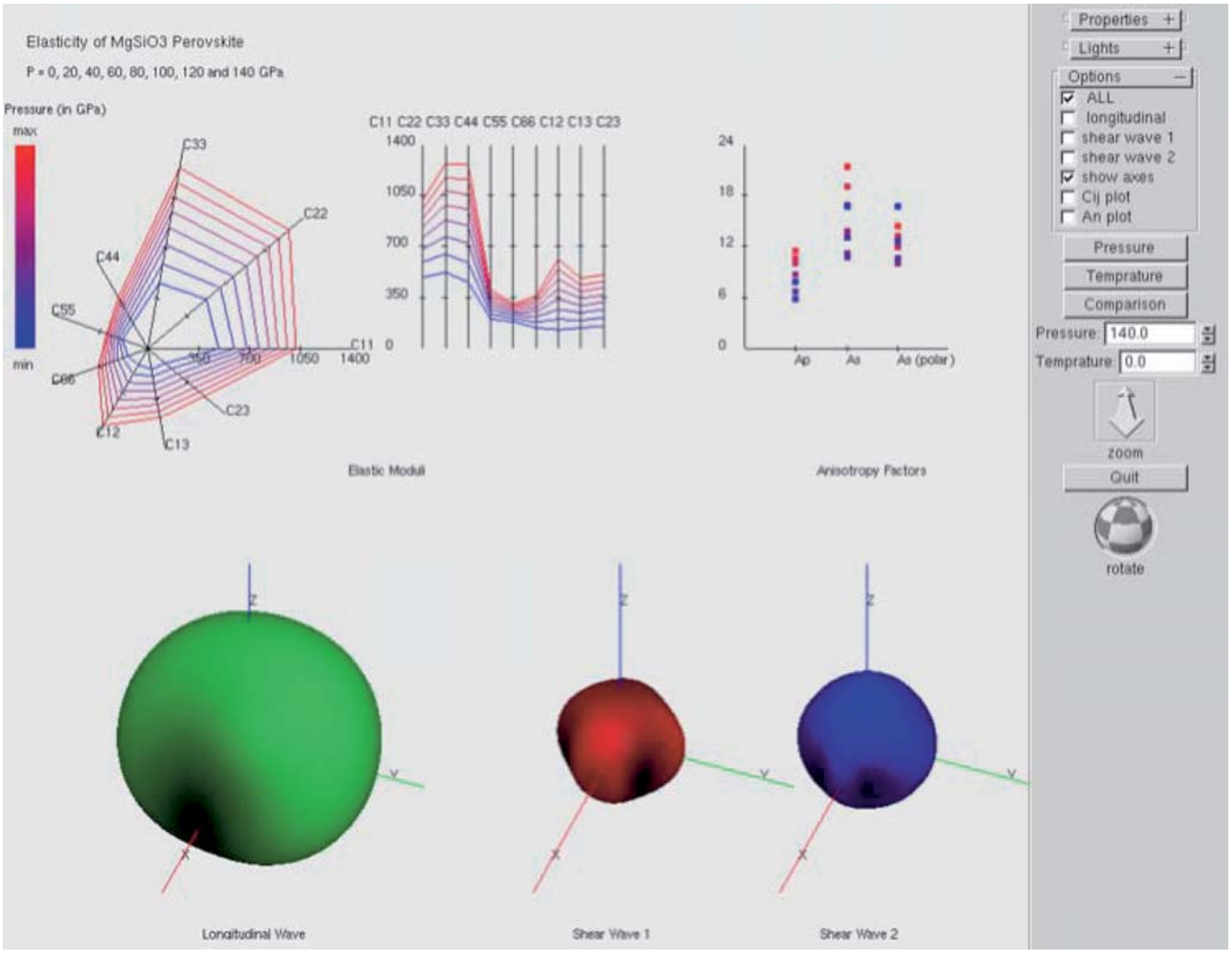

Fig. 7 Global visualization mode: elastic moduli and anisotropy factors of $MgSiO_3$ perovskite (Karki et al. 1997) are displayed as a function of pressure (P). Wave velocity surfaces are only shown at $P = 140$ GPa. The pressure range is indicated by the color variation from blue to red

vectors for those vertices. The above wave equation is then solved on the resulting fine set of the directional unit vectors in the 3D space. As a result, we have three sets of velocity data, one for longitudinal (P) and two for shear (S1 and S2) waves as a function of propagation direction.

The computed velocity-direction data are graphically displayed using the polygon-based surface rendering technique (Woo et al. 1999; Schroeder et al. 1997). This involves readjustment of the positions of the vertices on the surface of the icosahedron along the corresponding radial directions and hence use of distorted triangles. For each vertex, the unit vector is scaled by the magnitude of the velocity of a given wave type (P or S1 or S2) propagating along the direction of that vector. Thus re-positioned vertices represent the velocity-direction distribution in the 3D space; there are three such distributions, one for each wave type. Once a set of points (vertices) is thus generated, the data are displayed as a continuous surface by rendering the connected triangles with OpenGL (Fig. 5). Provided that the vertices are sufficiently close to each other, the resulting surfaces appear to be smooth.

Two approaches are used to enhance the three-dimensional view of the velocity surfaces. The first approach is shading which requires setting up an appropriate lighting environment and defining normals at vertices. OpenGL allows us to define the required light sources and material properties of the surface to be displayed. The required normal at each vertex is calculated using information about neighboring vertices. As such, lighting calculations are performed on a vertex-by-vertex basis to have smooth shading (Fig. 5). The second approach is scaled-coloring (the rightmost in Fig. 5) in which the color intensity at each point (vertex) is varied according to the magnitude of the velocity for a given wave type (X = P, S1 or S2):

$$I_X = \frac{V_X - V_X^{\min}}{V_X^{\max} - V_X^{\min}}$$

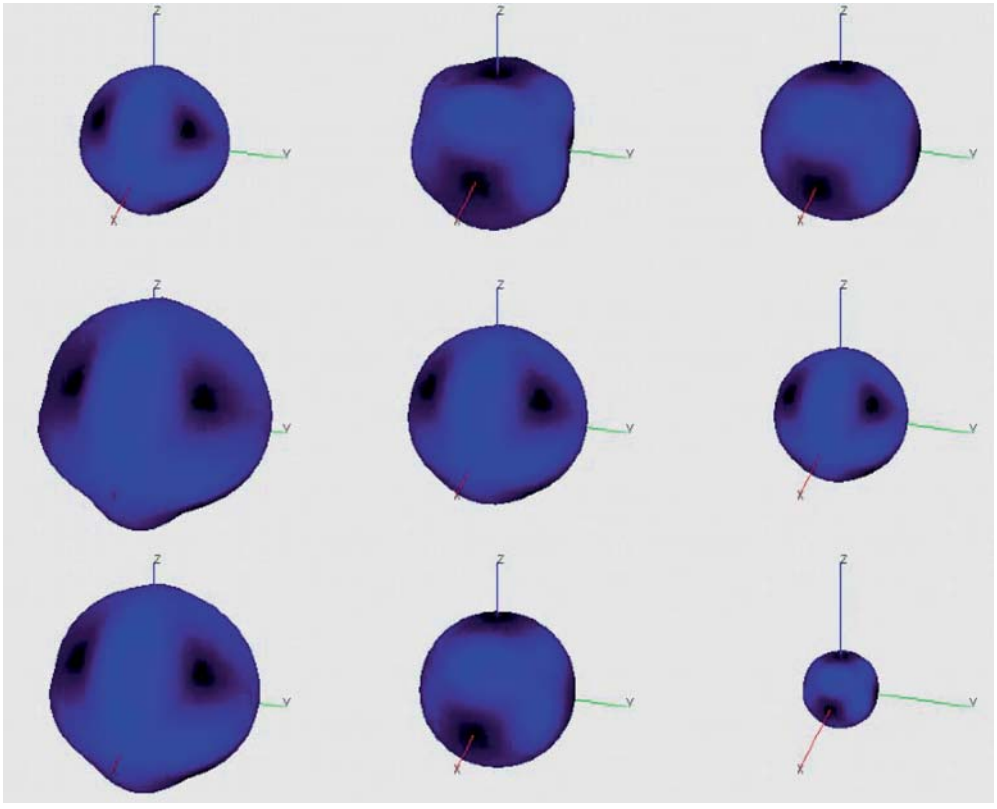

Fig. 8 Shear wave velocity surfaces of nine cubic crystals, which are, respectively, MgO, CaO, BaO, $CaSiO_3$, γ-Mg_2SiO_4, Fe_3O_4, $FeCr_2O_4$, FeS_2 and $Mg_3Al_2Si_3O_{12}$ from the left to right. Data are taken from the Elle Mineral Properties Database (2004). Note that x-, y- and z-axes are equivalent to the 100, 010 and 001 propagation direction, respectively

This restricts the color values of given type (red, blue or green) to the range of 0 to 1. Note that the lighting calculations are skipped in this case.

The velocity surfaces are represented by different colors: green for longitudinal wave, red for shear wave 1, and blue for shear wave 2, as shown in Fig. 6. Thus, the shape and brightness of the closed 3D surface together represent the velocity-direction distribution. The distance of each point on the surface from the center is proportional to the magnitude of the wave velocity for that point/direction. The color of each point on the surface is another indicator of the relative magnitude of the wave velocity at that point. Thus, darkest color represents the minimum value of the velocity, corresponding to vertex positions closest to the center, whereas the brightest color represents the maximum value and the corresponding vertices are farthest from the center. If the medium is isotropic, the velocity is independent of the propagation direction so the resulting velocity surface is perfectly spherical. However, in an anisotropic medium, the velocity surface deviates from the spherical shape as well as shows variation in the brightness of the surface.

We also visualize different anisotropy factors (see Karki et al. 2001). The azimuthal anisotropy factors for P and S waves which give a measure of velocity dependence on the propagation direction, can be defined by the following relations

$$A_P^{az} = \frac{V_P^{\max} - V_P^{\min}}{<V_P>} \times 100; A_S^{az} = \frac{V_S^{\max} - V_S^{\min}}{<V_S>} \times 100$$

where $< V_P >$ and $< V_S >$ are the isotropic velocities (that is, averaged over all propagation directions). For the shear waves, the polarization anisotropy can be calculated from the difference in velocities of two shear waves (S1 and S2) propagating in a given direction using

$$A_S^{po} = \frac{V_{S1} - V_{S2}}{<V_S>} \times 100.$$

The maximum polarization anisotropy occurs for the direction in which two shear wave velocities have the maximum difference. These parameters are displayed using the scatter plot technique for the longitudinal and shear waves.

Interactive user interface

Our scheme supports two visualization modes: First, it supports the global visualization mode, which is a simultaneous display of all properties including elastic moduli, anisotropy parameters and velocity surfaces (Fig. 7). Second, it supports the selective visualization mode, which displays individual properties (C_{ij} 's or velocity surfaces or anisotropy parameters) at a time, see Fig. 2, 3, 6 and 8. In both modes, pressure or temperature can be varied or different minerals can be chosen

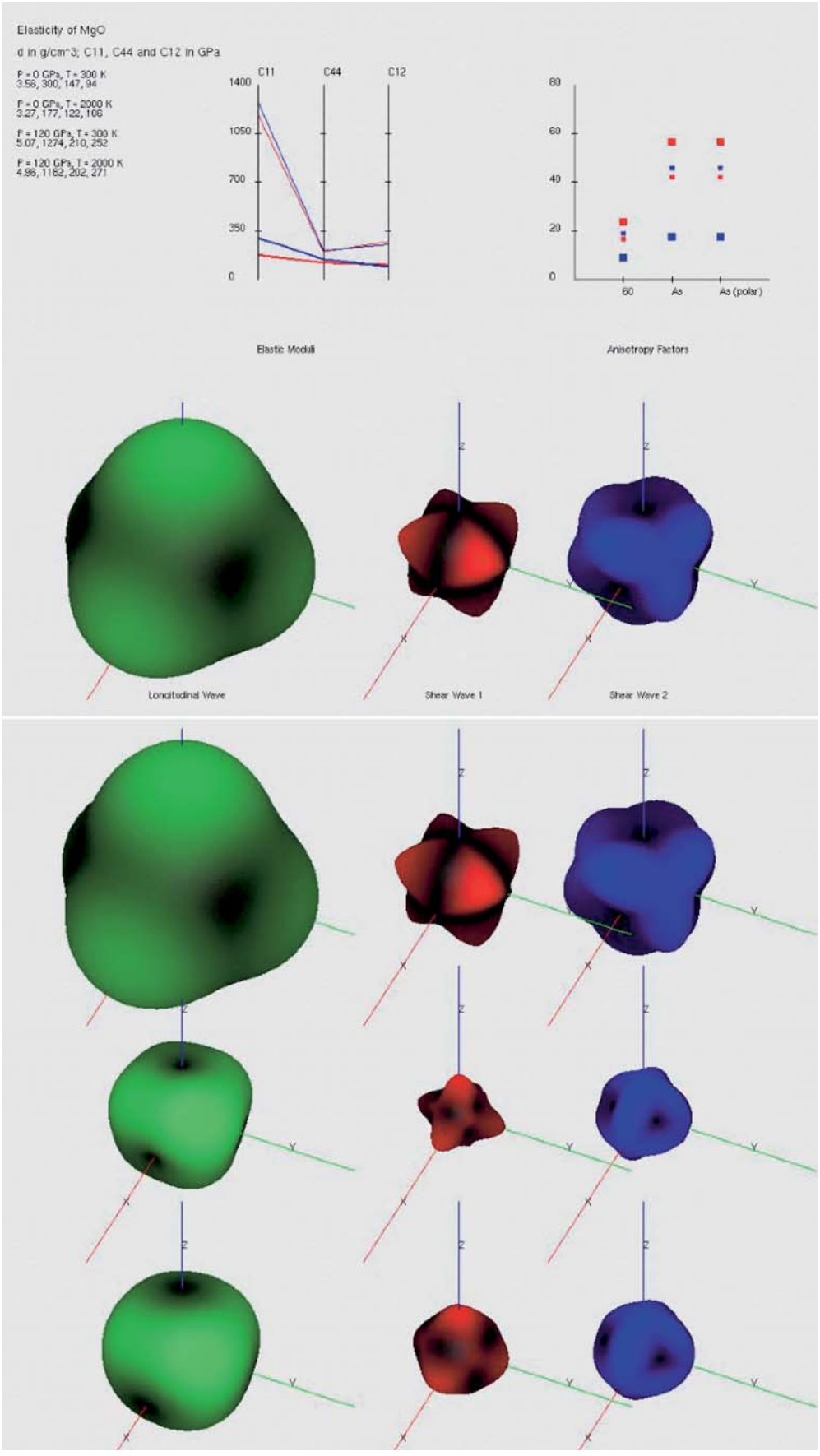

Fig. 9 Visualization of the effects of pressure and temperature on elasticity of MgO. *Upper part*: elastic moduli and anisotropy at 0 GPa are thick lines and big squares, respectively, and those at 120 GPa are thin lines and small squares, respectively. Blue and red are at 300 and 2000 K, respectively. Velocity surfaces are at 120 GPa and 2000 K. *Lower part*: from top to bottom are wave velocities at 120 GPa and 300 K, = GPa and 2000 K, and 0 GPa and 300 K

interactively. Additional options including rotation about an arbitrary axis and scaling by an arbitrary factor of the viewgraph are also provided. The user-interface is mouse driven, keyboard and/or menu-based; they are implemented using GLUT and GLUI libraries.

Figure 7 displays the pressure dependence of elasticity of orthorhombic $MgSiO_3$ perovskite using the theoretical data (Karki et al. 1997). The visualization system loads the input data (density and elastic constants) in full using the module **ReadData()** and uses them to compute velocity-direction data as a function of pressure incrementally. Only the first set of data (i.e. data at zero pressure) is displayed in the beginning. Pressure can then be changed using the right (to increase pressure) and left (to decrease pressure) arrows. Whenever the right/left arrow is pressed, the module **GenerateVelocities()** is called to compute velocity-direction distributions at the corresponding pressure (see Fig. 1). In the global visualization mode, velocity surfaces are displayed only at the current pressure whereas elastic moduli and anisotropy factors displayed at all pressures up to the current pressure. However, in the selective visualization mode, both display options (instantaneous and accumulated displays of data) are supported for all properties including velocity data. A keyboard interface allows us to toggle between two display modes. A similar mechanism is used to interactively control temperature and composition during visualization.

Applications

The elastic properties of several oxide and silicate minerals are visualized using the measured ambient data wherever available otherwise using the calculated data. Figure 2 and 3 display elastic moduli. The elasticity of minerals of all symmetry types (from cubic to triclinic) can be visualized using our system. The wave velocity surfaces of different minerals are found to vary in both size and shape implying a wide variation in the anisotropy with composition and phase. For instance, the velocity-direction surfaces of the cubic crystals clearly show the two distinct patterns in which the velocity maxima and minima are oppositely located for each type of wave. As shown by shear wave visualization of nine cubic crystals in Fig. 8, five minerals (MgO, $CaSiO_3$, γ-Mg_2SiO_4, Fe_3O_4, $FeCr_2O_4$) have one pattern whereas four minerals (CaO, BaO, FeS_2, $Mg_3Al_2Si_3O_{12}$) have an opposite pattern.

The effects of pressure and temperature on elasticity are visualized using the calculated elastic moduli of MgO (Karki et al. 1999) and $MgSiO_3$ perovskite (Karki et al. 1997; Wentzcovitch et al. 2004). The visualization clearly reveals that the anisotropy is strongly pressure dependent (Fig. 7 and 9): The maxima and minima of all velocity surfaces change their positions as the pressure is increased. For instance, the P- wave velocity surface of MgO has a minimum along [100] and a maximum along [111] at zero pressure but it has a minimum along [111] and a maximum along [100] at high pressure, as shown in Fig. 9. Similarly, the shape of both S-wave surfaces changes significantly with increasing pressure. The effects of temperature are relatively strong at zero pressure but become increasingly suppressed under pressure for both minerals.

Conclusion

The paper describes the design, implementation and application of a recently developed visualization system that enables a visually aided analysis of the existing large collections of mineral elasticity data. Our system allows us to successfully visualize multivariate elastic moduli themselves and the resulting anisotropic wave propagation as a function of composition, pressure and temperature. The graphical representation of data is performed using a combination of parallel coordinates, star plot, scatter plot and polygon-surface rendering techniques, which are implemented using OpenGL, GLUI and C++. This results in a highly portable and flexible interactive visualization system. At present, we have successfully visualized the elasticity of single crystalline minerals under the influence of pressure and temperature. In the future, we will extend the elasticity visualization to the cases of polycrystalline (e.g., transverse anisotropy) and multiphase composites. We will also make it web-enabled using a client-server framework and support remote analysis of the mineral elasticity data over the Internet.

Glossary

C++: a standard programming language developed at ATT Bell laboratories, which contains both procedural and object-oriented features.

GLUI: OpenGL user interface software.

Lighting: The process of computing the color of a vertex based on the current lights, material properties, and lighting-model modes.

Normal: a three-component plane equation that defines the angular orientation of a plane or surface and used in lighting calculations.

OpenGL: an interactive computer graphics system that allows programmers to write programs that access graphics hardware.

Rendering: conversion of primitives specified in object coordinates to an image in the frame buffer.

Voigt symmetry: allows replacement of a pair of Cartesian indices (i,j) by single index m according to the scheme:

ij = 11 22 33 32 or 23 31 or 13 21 or 12

m = 1 2 3 4 5 6

Acknowledgements The authors would like to thank G. Erlebacher (Florida State University), SS Iyengar (Louisiana State University), L Stixrude (University of Michigan), and RM Wentzcovitch and

DA Yuen (University of Minnesota) for carefully reading the manuscript and providing useful suggestions. They also thank Paul Miller for his help in the initial implementation of the project. This work is supported by National Science Foundation EAR 0347204.

References

Dzwinel W, Yuen DA, Kaneko YJBD, Boryczko K, Ben-Zion Y (2003) Multi-resolution clustering analysis and 3D visualization of multitudinous synthetic earthquakes. Visual Geosciences 8:12–25

Erlebacher G, Yuen DA, Dubuffet F (2001) Current trends and demands in visualization in the geosciences. Elect Geosci 4

Erlebacher G, Yuen DA, Dubuffet F (2002) Case study: visualization and analysis of high Rayleigh number–3D convection in the Earth's mantle. Proceedings of IEEE Visualization, pp 529–532

Karki BB, Stixrude l, Warren MC, Clark SJ, Ackland GJ, Crain J (1997) Elastic properties of orthorhombic $MgSiO_3$ perovskite at lower mantle pressures. Am Mineral 82:635–638

Karki BB, Stixrude L, Wentzcovitch RM (2001) Elastic properties of major materials of earth's mantle from first principles. Rev Geophys 39:507–534

Karki BB, Wentzcovitch RM, de Gironcoli S, Baroni S (1999) First principles determination elastic anisotropy and wave velocities of MgO at lower mantle conditions. Science 286:1705–1707

Liebermann RC, Li B (1998) Elasticity at high pressures and temperatures. Rev Mineral 37:459–492

Musgrave MJP (1970) Crystal acoustics, Holden-Day, San Francisco

Oganov AR, Brodholt JP, Price GD (2001) The elastic constants of $MgSiO_3$ perovskite at pressures and temperatures of the Earth's mantle. Nature 411:934–937

Schroeder W, Martin K, Lorensen B (1997) Visualization toolkit: an object-oriented approach to 3D graphics. Prentice Hall

Sinogeikin SV, Zhang J, Bass JD (2004) Elasticity of single crystal and polycrystalline $MgSiO_3$ perovskite by Brillouin spectroscopy. Geophys Res Lett 31, No. GL019559

The Elle Mineral Properties Database (2004) http://www.microstructure.uni-tuebingen.de/mindb

Voigt W (1928) Lehrbuch der Kristallphysik, Teubner, Leipzig

Wang Y, Erlebacher G, Garbow ZA, Yuen DA (2004) Web-based service of a visualization package "Amira" in the geosciences

Wentzcovitch RM, Karki BB, Cococcioni M, de Gironcoli S (2004) Elasticity and wave velocities of $MgSiO_3$ perovskite: insight into lower mantle. Phys Rev Lett 92: No. 018501

Woo M, Neider J, Davis T, Shreiner D (1999) OpenGL programming guide: the official guide to learning OpenGL. Addison-Wesley